Biomaterials Advances 154 (2023) 213590

Contents lists available at ScienceDirect

Biomaterials Advances

journal homepage: www.journals.elsevier.com/materials-science-and-engineering-c

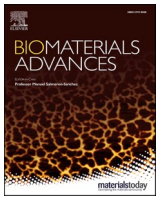

Electromechanical and biological evaluations of $0.94Bi_{0.5}Na_{0.5}TiO_3$–$0.06BaTiO_3$ as a lead-free piezoceramic for implantable bioelectronics

Thomas A.G. Hall [a], Konstantinos Theodoridis [a], Stylianos Kechagias [a], Nupur Kohli [a,b], Christelle Denonville [c], Per Martin Rørvik [c], Frederic Cegla [d], Richard J. van Arkel [a,*]

[a] Biomechanics Group, Department of Mechanical Engineering, Imperial College London, UK
[b] Biomedical Engineering Department, Khalifa University, United Arab Emirates
[c] Thin Film and Membrane Technology, Sustainable Energy Technology, SINTEF Industry, Norway
[d] Non-Destructive Evaluation Group, Department of Mechanical Engineering, Imperial College London, UK

ARTICLE INFO

Keywords:
Piezoelectricity
Biomedical implants
Energy harvesting
Wireless power transfer
Cytotoxicity
Electroactive implants

ABSTRACT

Smart implantable electronic medical devices are being developed to deliver healthcare that is more connected, personalised, and precise. Many of these implantables rely on piezoceramics for sensing, communication, energy autonomy, and biological stimulation, but the piezoceramics with the strongest piezoelectric coefficients are almost exclusively lead-based. In this article, we evaluate the electromechanical and biological characteristics of a lead-free alternative, $0.94Bi_{0.5}Na_{0.5}TiO_3$–$0.06BaTiO_3$ (BNT-6BT), manufactured via two synthesis routes: the conventional solid-state method (PIC700) and tape casting (TC-BNT-6BT). The BNT-6BT materials exhibited soft piezoelectric properties, with d_{33} piezoelectric coefficients that were inferior to commonly used PZT (PIC700: 116 pC/N; TC-BNT-6BT: 121 pC/N; PZT-5A: 400 pC/N). The material may be viable as a lead-free substitute for soft PZT where moderate performance losses up to 10 dB are tolerable, such as pressure sensing and pulse-echo measurement. No short-term harmful biological effects of BNT-6BT were detected and the material was conducive to the proliferation of MC3T3-E1 murine preosteoblasts. BNT-6BT could therefore be a viable material for electroactive implants and implantable electronics without the need for hermetic sealing.

1. Introduction

Advances in microelectronics, wireless networking protocols, and informatics are driving a new generation of Implantable Electronic Medical Devices (IEMDs) that are smarter, more capable, and more pervasive. Many functions of existing or emerging systems rely on piezoceramics: acoustic sensing in fully implantable cochlear implants [1]; wireless power transfer to therapeutic devices such as cardiac pacemakers [2], tumour photosensitisers [3] and neurostimulators [4]; wireless data transfer to and from neural interfaces [5,6]; and energy harvesting from physiological motion in the heart, lungs, and diaphragm [7]. The naturally occurring piezoelectricity of bone has been implicated in its healing response [8]: piezoceramics have therefore also been suggested as electroactive, power-source-independent biomaterials for supraphysiological tissue regeneration [9]. Injectable piezoceramic nanocrystals are also being investigated as catalysts for ultrasound-driven tumour therapies: mechanical stimulation of the nanocrystals has been shown to produce tumour-eradicating reactive oxygen species in in vivo xenograft models [10,11].

Historically, the best performing piezoceramics have been lead-based, principally lead zirconate titanate (PZT), but lead is highly toxic even in small doses [12]. EU legislation [13] has led to lead-based piezoceramics being phased out across many industry sectors and has fostered research into lead-free alternatives [14]. All medical devices were exempt when the legislation was first introduced, but the scope has been narrowing – the exemption for PZT-containing in vitro diagnostic equipment will lapse in 2023 [13] – and is expected to narrow further.

There are currently three families of lead-free piezoceramic materials that are considered candidates to replace PZT, which are based on potassium sodium niobate (KNN) [15,16], barium titanate (BT) [17], and bismuth sodium titanate (BNT) [16]. Of these families, the excellent piezoelectric properties of KNN-based piezoceramics incited current

* Corresponding author.
E-mail address: r.vanarkel@imperial.ac.uk (R.J. van Arkel).

https://doi.org/10.1016/j.bioadv.2023.213590
Received 15 February 2023; Received in revised form 1 August 2023; Accepted 13 August 2023
Available online 14 August 2023

lead-free research interest [18], and this family has in turn been the subject of intense development efforts [15]. However, large-scale preparation and processing of KNN-based piezoceramics is more challenging than current lead-based piezoceramics [16,19,20], and commercial translation of KNN-based piezoceramics has so far lagged behind research progress [21]. Within the BT-based ceramic family, calcium- and zirconium-doped barium titanate (BCZT) is of particular interest due to its high piezoelectric coefficients [17]. Its poor thermal stability, which is not detrimental to medical applications, and challenges in piezoceramic synthesis has limited commercial uptake of BT-based piezoceramics [19]. BNT-based piezoceramics demonstrate more modest piezoelectric properties than the KNN- and BT-based families [19], but thermal behaviour is more stable than BT-based piezoceramics. Moreover, BNT-based piezoceramics can be manufactured by the well-established techniques used for the production of commonly used ceramics, such as PZT [16]. In the BNT-based family, BT-doped BNT demonstrates the highest piezoelectric coefficients around the stoichiometric ratio $0.94Bi_{0.5}Na_{0.5}TiO_3$–$0.06BaTiO_3$ (BNT-6BT) due to a favourable lattice transition from rhombohedral to tetragonal phase [22]. BNT-6BT has therefore received considerable research interest, including for biomedical applications such as high-frequency ultrasound transducers [23].

In this article, the promising BNT-6BT material is characterised to determine its suitability for deployment in implantable electronics and electroactive implants. Two fabrication techniques are considered: the conventional solid-state sintering method and tape casting with lamination. The conventional ceramic method is well suited to the bulk manufacture of disc and plate transducers, which can be used in applications like wireless power transfer, whilst the tape casting technique is suited to the manufacture of multilayer actuation devices with reduced operating voltages. The electromechanical properties of ceramics from both fabrication techniques are characterised and contextualised with figures of merit for implant-relevant applications: sensing, actuation, stimulation, energy harvesting, and pulse-echo measurement. Furthermore, the cytotoxicity and biocompatibility of BNT-6BT were assessed to determine its suitability for in vivo applications.

2. Materials and methods

2.1. Specimens and fabrication

BNT-6BT piezoceramics from two fabrication techniques were investigated: the first specimens (PIC700) were a commercial material manufactured by the conventional ceramic method (PI Ceramic, Germany) whilst the second specimens (TC-BNT-6BT) were synthesised by tape casting with lamination. PIC700 samples were sintered and poled as a bulk material in an oil path; samples were then cut from the bulk material and lapped to the specified geometries (Ø10 × 1.25 mm^3 discs and 5 × 5 × 0.325 mm^3 plates) and silver electrodes were applied.

TC-BNT-6BT samples were made from ceramic powder manufactured by spray pyrolysis (CerPoTech, Norway). Self-standing tapes of BNT-6BT were cast to a final thickness of 0.2 mm after drying using an alcohol-based slurry. After drying in ambient air, laminated films were made by pressing at room temperature to obtain a final thickness of 0.9 mm. The dried tapes and the laminated films were cut and sintered at 1150 °C in air for 2 h: plates with dimensions of 5 × 5 × 0.9 mm^3 and 5 × 5 × 0.2 mm^3 were produced. Electrodes were applied using silver lacquer and samples were annealed at 700 °C for four hours before being poled in silicone oil at 3 kV/mm at 150 °C for 30 min and field-cooled to below 40 °C.

Samples of a commercial PZT material (NCE51, Noliac, Denmark) with dimensions of 5 × 5 × 0.5 mm^3 were used as a comparator to the BNT-6BT samples for the in vitro cytotoxicity testing.

2.2. Electromechanical characterisation

Electromechanical properties of the bulk-manufactured and tape-cast specimens were measured according to European standard EN 50324–2:2002 [24]. Impedance measurements around each resonance were acquired using a precision impedance analyser (4294A, Agilent, USA) at high bandwidth with sixteen averages per measurement. Relationships between resonant frequency pairs were used to calculate coupling factors and the dielectric, elastic, and piezoelectric constants.

Figures of merit were used to determine suitability of the characterised BNT-6BT specimens for implant-relevant applications: actuation, stimulation, sensing, energy harvesting, and pulse-echo measurement. These figures of merit were then referenced against current PZT-based piezoceramics and lead-free alternatives (Appendix: Table A.1).

High piezoelectric charge/strain coefficients ($d_{i\alpha}$), which cause materials to exhibit high displacement in response to applied voltage (converse piezoelectric effect), were regarded as appropriate for actuator materials [25]. Materials with high piezoelectric voltage coefficients ($g_{i\alpha}$) exhibit high output voltages generation in response to applied stress (direct piezoelectric effect). Materials with high $d_{i\alpha}{\cdot}g_{i\alpha}$ were regarded as ideal sensors [26].

Two different figures of merit were used for off-resonance and on-resonance piezoelectric energy harvesting [27], which corresponded to energy harvesting at low frequencies (<1 kHz; e.g. physiological motion) and high frequencies (>100 kHz; e.g. acoustic power transfer). In the thickness-extension mode, these figures of merit (FOMs) were

$$\mathrm{FOM}_{\mathrm{off-res.}} = \frac{d_{33}{\cdot}g_{33}}{tan\delta_{\mathrm{E}}} \tag{1}$$

$$\mathrm{FOM}_{\mathrm{on-res.}} = k_t^2{\cdot}Q_{\mathrm{M}} \tag{2}$$

where $tan\delta_{\mathrm{E}}$ was the dielectric loss tangent, k_t was the thickness-mode piezoelectric coupling coefficient, and Q_M was the mechanical quality factor.

For pulse-echo transducers, the transmission efficiency and receiver sensitivity parameters (TP and RP respectively) in the thickness-extension mode were used as figures of merit [28]:

$$\mathrm{TP} = \frac{k_t}{1-k_t^2}\sqrt{\frac{\varepsilon_{33}^S}{c_{33}^D}}, \tag{3}$$

$$\mathrm{RP} = \frac{k_t}{\sqrt{c_{33}^D\varepsilon_{33}^S}}, \tag{4}$$

where ε_{33}^S was the permittivity at constant strain and c_{33}^D was the stiffness at constant dielectric displacement, both in the poling direction.

2.3. Biological characterisation

2.3.1. Cytotoxicity and cell proliferation

The in vitro cytotoxicity of BNT-6BT was evaluated according to ISO 10993-5:2009 [29], including both direct tests for cell ongrowth and indirect tests for leaching. Poled, non-electroded PIC700 and unpoled, non-electroded TC-BNT-6BT samples (both $n = 3$) were sterilised by immersion in 70 % ethanol solution (30 mins) and irradiation by UV light (30 mins on each side). In the direct tests, murine preosteoblasts from the MC3T3-E1 cell line (ATCC CRL-2593) were seeded directly on the samples (passage 1) at a density of 50,000 cells/cm^2 and cultured for 24 h (37 °C; 5 % CO_2; 21 % O_2) in basic cell culture medium: MEM (Gibco™, Thermo Fisher Scientific, USA) supplemented with 10 % foetal bovine serum (Gibco™, Thermo Fisher Scientific, USA) and 1 % penicillin-streptomycin (Gibco™, Thermo Fisher Scientific, USA). In the indirect tests, samples were incubated in media for 24 h at 37 °C prior to testing, and 12,500 cells/well were cultured in serial dilutions of the extracted media (0 %, 25 %, 50 % and 100 %). PZT samples (Noliac

NCE51; 5 × 5 × 0.5 mm^3; $n = 3$) were used as a comparator, and media with 10 % DMSO (ATCC 4-X) was used a cytotoxic control. Fluorescence readings (λ_{ex}: 530 nm; λ_{em}: 590 nm) for cell metabolic activity were acquired in triplicate after 30 min incubation with alamarBlue Cell Viability Reagent (ThermoFisher DAL1025) according to the manufacturer's instructions. These measurements of metabolic activity were repeated again after 5 and 9 days with the PIC700, the PZT reference material, and the blank media to record cell proliferation. The pH level of each sample was monitored throughout culture.

2.3.2. In vitro culture

Murine preosteoblasts from the MC3T3-E1 cell line (ATCC CRL-2593) were proliferated until passage three in basic cell culture medium: MEM (Gibco™, Thermo Fisher Scientific, USA) supplemented with 10 % foetal bovine serum (ATCC 30–2020) and 1 % penicillin-streptomycin (Gibco™, Thermo Fisher Scientific, USA). At 90 % confluency on the final passage (Fig. 1), the cells were trypsinised and centrifuged for 5 min at 1200 rpm within 15 ml falcon tubes. After centrifuge, the cell pellet was extracted and measured with a haemocytometer, and 5000 cells/cm^2 were seeded directly onto PIC700 BNT-6BT samples ($n = 3$). Specimens with cells were left for 40 min inside the incubator to allow cells to adhere to the ceramic surface, before 1 ml of basic cell culture medium was added to each well. Specimens were cultured in 24-well plates for 7, 14, and 21 days in standard normoxic conditions (37 °C; 5 % CO_2; 21 % O_2), and cell culture medium was replaced every 3–4 days as needed.

Viability was determined at each timepoint by staining samples with Calcein-AM/Ethidium homodimer (Biotium, USA) according to the manufacturer's instructions. After the addition of both dyes, the samples were maintained in the dark at room temperature for 30 min, washed with phosphate buffered saline, and imaged using an upright confocal microscope (Leica Microsystems, Germany). Fifteen serial sections were captured as z-stack images using the Leica software.

After confocal imaging, samples were fixed in 2.5 % glutaraldehyde with 0.1 M phosphate buffer (pH 7.4) overnight, dehydrated through a series of ethanol solutions (20–100 %; 7 min per solution), and air-dried for analysis. Samples were then sputter-coated with chromium (thickness: 15 nm) and imaged using a scanning electron microscope (TESCAN MIRA, Czechia) for signs of cellular ongrowth.

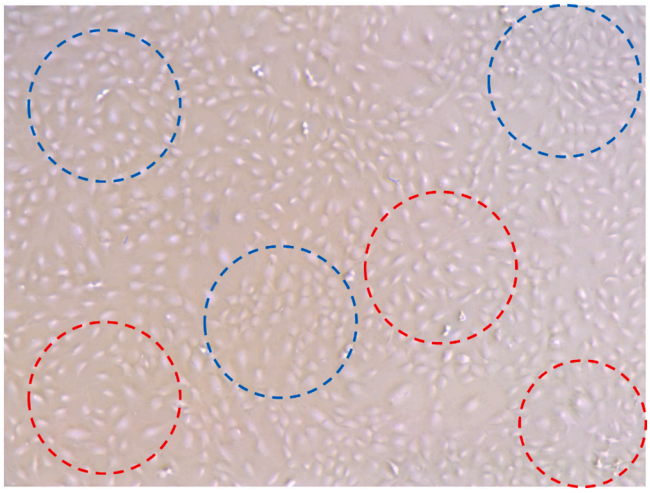

Fig. 1. Murine preosteoblast cells at 90 % confluency on the final passage for the in vitro biocompatibility test: cells were ellipsoidal when clustered (blue circles) and more elongated with protruding lamellipodia when more isolated (red circles). (For interpretation of the references to colour in this figure legend, the reader is referred to the web version of this article.)

2.3.3. Ex vivo culture

The cytotoxicity of PIC700 BNT-6BT specimens was evaluated in living bone using an ex vivo bioreactor model as an alternative to early-stage animal testing [30]. Fresh trabecular bone cores (Ø10 mm × 5 mm; $n = 6$) were extracted from distal porcine femur in a sterile hood using a sterilised surgical sagittal and hole saw. The cores were then washed in Dulbecco's phosphate-buffered saline (DPBS; Gibco™, Thermo Fisher Scientific, USA) with 1 % penicillin/streptomycin (Gibco™, Thermo Fisher Scientific, USA) and vortexed for 30 s to reduce cutting debris. An incision was made into each of the bone cores with a scalpel through the midplane of the cylinder from its axis to its circumference. PIC700 plates, sterilised in accordance with Section 2.3, were then press-fit into the incisions. The remaining cores ($n = 2$) were incised without implantation as controls. All bone cores were then incubated (37 °C; 5 % CO_2; normoxic) in cell culture medium, which consisted of DMEM/F-12 with HEPES (Gibco™, Thermo Fisher Scientific, USA) plus 10 % foetal bovine serum (Gibco™, Thermo Fisher Scientific, USA) and 1 % penicillin/streptomycin (Gibco™, Thermo Fisher Scientific, USA) and was replaced every seven days. All bone cores were culturing within the incubator within five hours of euthanisation. The culture was terminated after 28 days.

Each bone core was stained with Calcein-AM/Ethidium homodimer (Biotium, USA) according to the same process as Section 2.3.2, and samples were imaged for cell viability using an upright confocal fluorescence microscope (Leica Microsystems, Germany). Images were acquired from the surface of the piezoceramic, from bone tissue adjacent to the piezoceramic, and in the bulk of the tissue (enabled with an additional incision made post-staining). Approximately 15 serial sections of the tissue's live/dead cells were captured as z-stack images and merged using the Leica software.

Research was registered in accordance with the host institution's policy for lab-based research with animal tissue. Tissue was sourced as a waste material from pigs that were euthanised for unrelated research that did not affect bone metabolism or healing.

3. Results

3.1. Electromechanical characterisation

Piezoelectric coefficients for the bulk-manufactured and tape-cast BNT-6BT specimens (PIC700 and TC-BNT-6BT respectively) were near-equivalent. Referencing the materials for sensing, charge coefficients (d_{33}) were ~ 10 dB lower than a standard PZT material (PZT-5A) for the same application, whilst voltage coefficients (g_{33}) were similar (Table 1; Fig. 2a). Performance in sensing applications was

Table 1
Electromechanical characterisation of PIC700 in the planar and thickness-extension modes.

	Symbol	PIC700	TC-BNT-6BT	Units
Dielectric Properties				
Relative permittivity	$\varepsilon_{33}^T/\varepsilon_0$	648	638	–
Dielectric loss tangent	$tan\delta_E$	205	300	$\times 10^{-4}$
Piezoelectric Properties				
Electromechanical coupling factors	k_p	0.088	0.15	–
	k_t	0.401	0.22	–
Piezoelectric constants	d_{33}	116	121	pC/N
	g_{33}	20.3	21	mV·m/N
Mechanical Properties				
Elastic compliances	c_{33}^D	10.1	–	$\times 10^{10}$ N/m^2
	s_{33}^E	12.3	–	$\times 10^{-12}$ m^2/N
Mechanical loss tangent	$tan\delta_M$	76	104	$\times 10^{-4}$

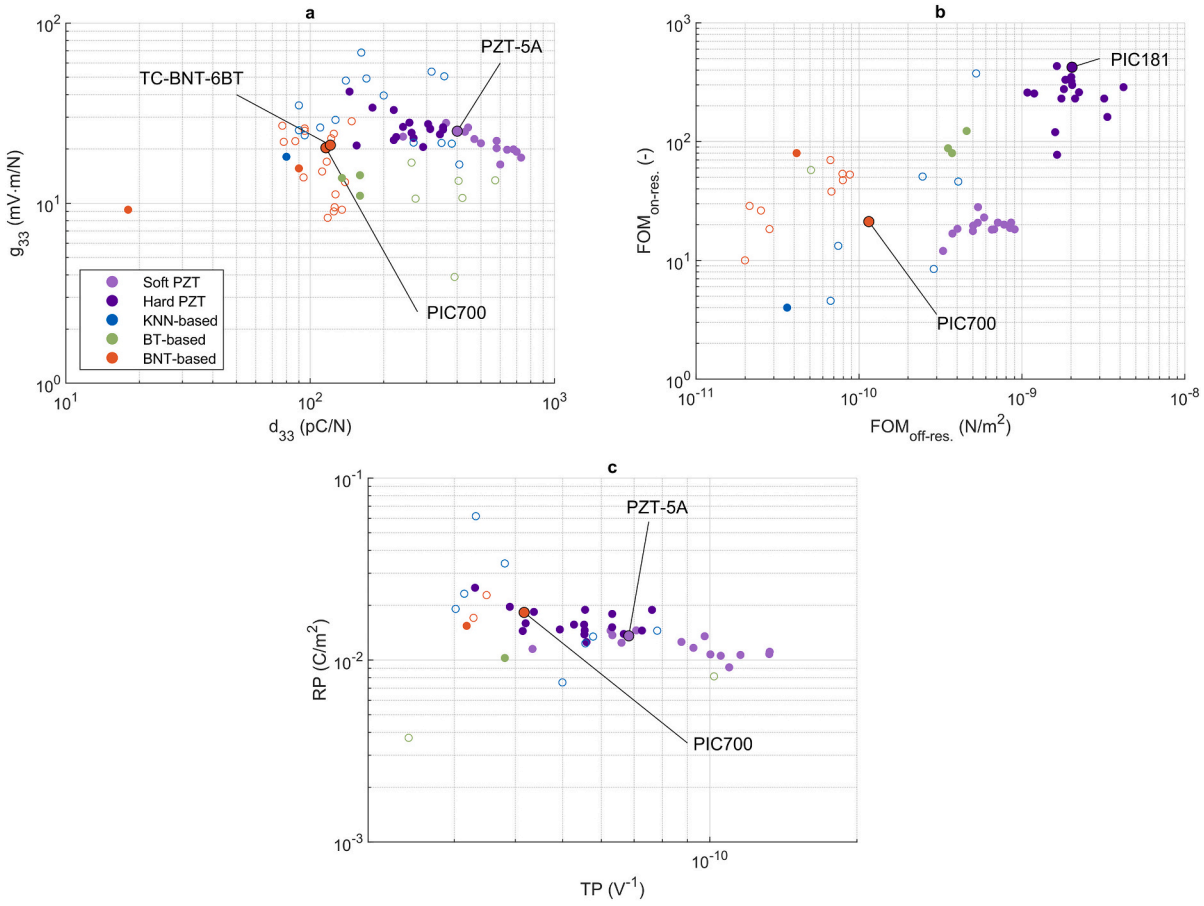

Fig. 2. Figures of merit for BNT-6BT versus conventional PZT-based and other lead-free piezoceramics (● commercial; ○ research): (a) piezoelectric charge and voltage coefficients; (b) off- and on-resonant energy harvesting performance; and (c) transmission efficiency and receiver sensitivity. Performance is best in the top right corner of each plot and decreases as either the x- or y- parameter decreases.
Data sources: [50–82]. [52–84].

comparable to the other lead-free alternatives: KNN-based and BT-based piezoceramics. Figures of merit for BNT-6BT (PIC700) were substantially lower in off-resonant (−24.9 dB) and on-resonant (−31 dB) energy harvesting applications compared to a standard PZT material (PIC181; Fig. 2b). Performance metrics in energy harvesting applications were comparable to KNN-based piezoceramics but considerably lower than BT-based piezoceramics (Fig. 2b; 10–15 dB in both modes). Transmit efficiency and receiver sensitivity parameters for pulse-echo transducers in the thickness-extension mode were similar for all piezoceramic families (Fig. 2c): BNT-6BT (PIC700) was at the lower end of the range of PZT transmit efficiency parameters with a performance deficit of 8 dB to the best-performing PZT material.

3.2. Biological characterisation

3.2.1. Cytotoxicity and cell proliferation

The viability of MC3T3-E1 murine preosteoblasts was above the ISO 10993-5:2009 cytotoxicity threshold (70 % of the 24-hour baseline value) in all assays of BNT-6BT specimens, for both manufacturing methods, and for both the indirect elution and the direct contact tests (Fig. 3a, −b & -e; 84–127 % viability). The same was true for the PZT reference material (Fig. 3c & -e; 86–134 %), but cell viability did reduce to 37 % in the cytotoxic control (10 % DMSO; Fig. 3d; $p < 0.001$). The MC3T3-E1 cells proliferated from day 1 through to day 9 in the extended direct contact cultures with the BNT-6BT (PIC700; Fig. 4; 292 % proliferation; $p < 0.001$) and PZT (NCE51; 338 %; $p < 0.001$) specimens, though proliferation by day 9 was 47 % slower than the cells in blank media (552 %; $p < 0.001$). The pH in all tests remained neutral.

3.2.2. In vitro culture

In all phases of the 21-day in vitro culture, the MC3T3-E1 cells demonstrated typical morphologies and growing behaviour, with high viability and proliferation of cells up to 100 % confluence on the BNT-6BT piezoceramic surface by this time point (Fig. 5). Flattened cells with lamellipodia were seen growing in small clusters on the BNT-6BT surface after seven days of culture (Fig. 6a & -d); cell density had increased and small deposits (~50 μm in thickness) of extracellular matrix were observed on day 14 (Fig. 6b & -e); and continued proliferation through to day 21 had resulted in dense cell coverage and further deposition of immature extracellular matrix on the piezoceramic surface (Fig. 6c & -f).

3.2.3. Ex vivo culture

After 28 days of ex vivo culture, organic tissue (~100 μm) was observed on the implanted BNT-6BT specimens but there was no evidence of cell proliferation onto the piezoceramic (Fig. 7a). High viability was maintained in the cancellous bone tissue adjacent to the implant (Fig. 7b) and in the bulk tissue (Fig. 7c), indicating no considerable harmful effect of BNT-6BT on bone viability in the first 28 days of implantation.

4. Discussion

This study presents the most comprehensive assessment of BNT-6BT as a lead-free piezoceramic for biomedical implant applications, investigating BNT-6BT from two synthesis routes, solid state (PIC700) and tape casting with lamination (TC-BNT-6BT), and considering several

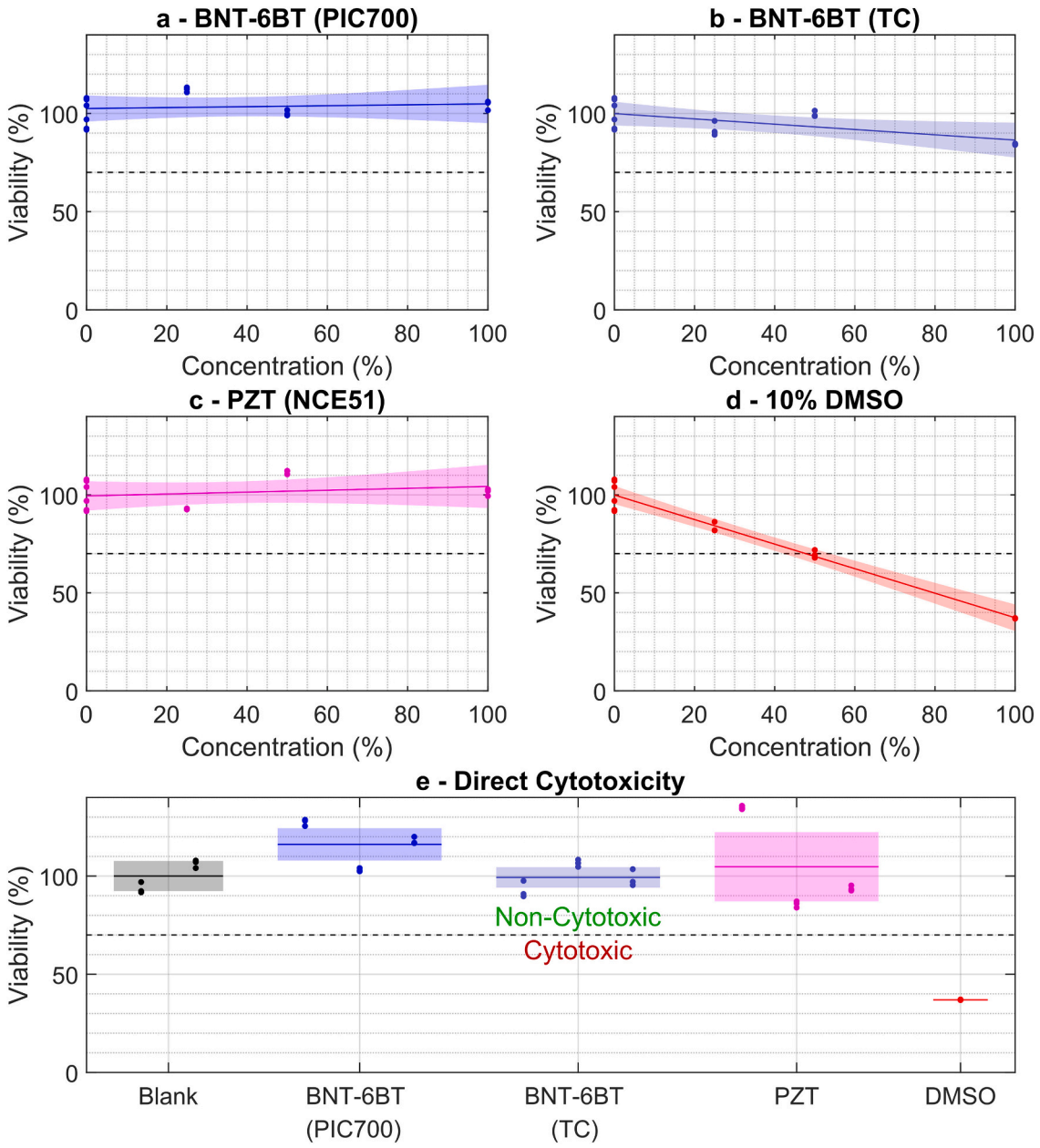

Fig. 3. ISO 10993-5 indirect cytotoxicity testing of (a) bulk-manufactured BNT-6BT (PIC700) and (b) tape-cast BNT-6BT compared to (c) PZT (NCE51) and (d) cytotoxic control (10 % DMSO), and (e) direct cytotoxicity testing for all samples.

applications, including sensing, power transfer, and tissue regeneration. The electromechanical and biological properties of both materials were evaluated with reference to conventional PZT materials and leading lead-free alternatives: KNN- and BT-based piezoceramics.

The measured piezoelectric coefficients of the bulk-manufactured BNT-6BT (PIC700; d_{33}: 116 pC/N: g_{33}: 20.3 mV·m/N) were consistent with results from two other publications [31,32]. Piezoelectric coefficients for the tape-cast BNT-6BT (TC-BNT-6BT; d_{33}: 121 pC/N: g_{33}: 21 mV·m/N) were concordant with the bulk-manufactured piezoceramic, and similar piezoelectric performance should be expected. These properties were weaker than standard PZT materials (d_{33}: ~400 pC/N; g_{33}: ~25 mV·m/N) but comparable to undoped lead-free piezoceramics: KNN (d_{33}: ~100 pC/N; g_{33}: ~25 mV·m/N) and BT (d_{33}: ~150 pC/N; g_{33}: ~15 mV·m/N) (Appendix: Table A.1). Doped KNN- and BT-based piezoceramics with higher coefficients have been produced, notably BCZT (d_{33}: ~500 pC/N; g_{33}: ~10 mV·m/N), but these materials are yet to be commercialised.

Figures of merit indicated that performance losses of ~10 dB would be associated with the substitution of standard PZT materials with BNT-6BT in sensing and pulse-echo measurement applications, though performance was comparable to other undoped lead-free piezoceramics and may be tolerable in some implantable electronic systems. BNT-6BT was shown to be less suitable for energy harvesting systems, on-resonant or off-resonant, with figures of merit predicting performance losses up to 30 dB. The voltage coefficient (g_{33}) of BNT-6BT is comparable to PZT and other lead-free materials: BNT-6BT may therefore be a good candidate for investigating electrically stimulated tissue regeneration with higher piezoelectric coefficients [9].

The short-term cytological properties of BNT-6BT appear promising: cell viability was above the cytotoxicity threshold in both the ISO 10993-5 indirect elution and direct contact assays with both BNT-6BT materials. Additionally, no effect on cell viability was detected when poled PIC700 was implanted in bone and cultured ex vivo. These experiments on murine preosteoblast cells (MC3T3-E1) and porcine bone

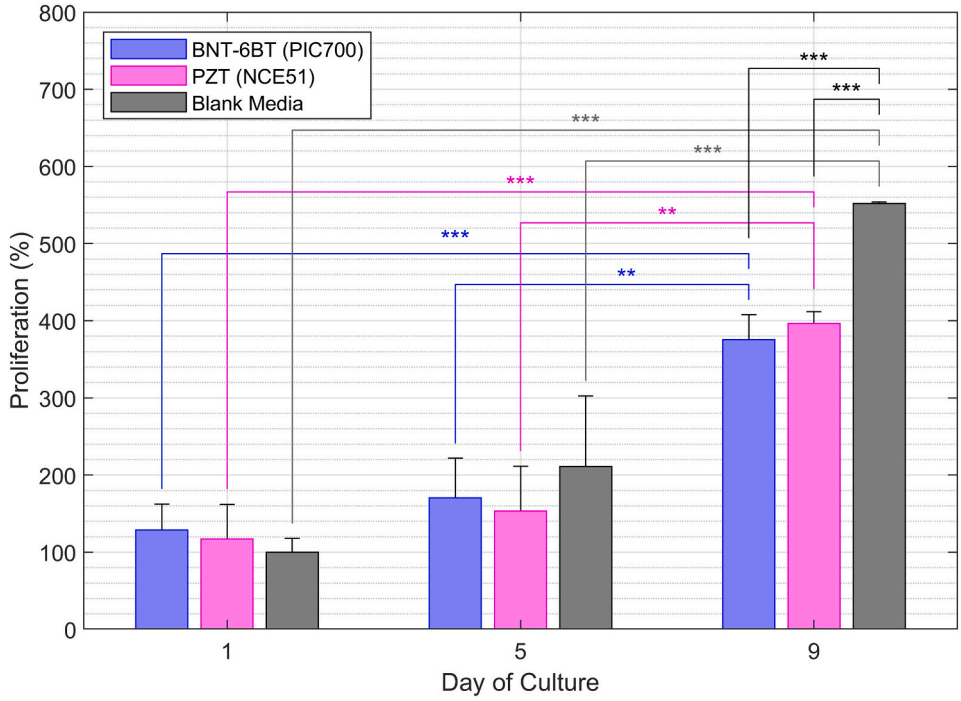

Fig. 4. Metabolic activity of cells in extended direct contact cultures with BNT-6BT (PIC700), PZT and blank media, normalised by day-1 blank media readings (**: $p < 0.005$; ***: $p < 0.001$).

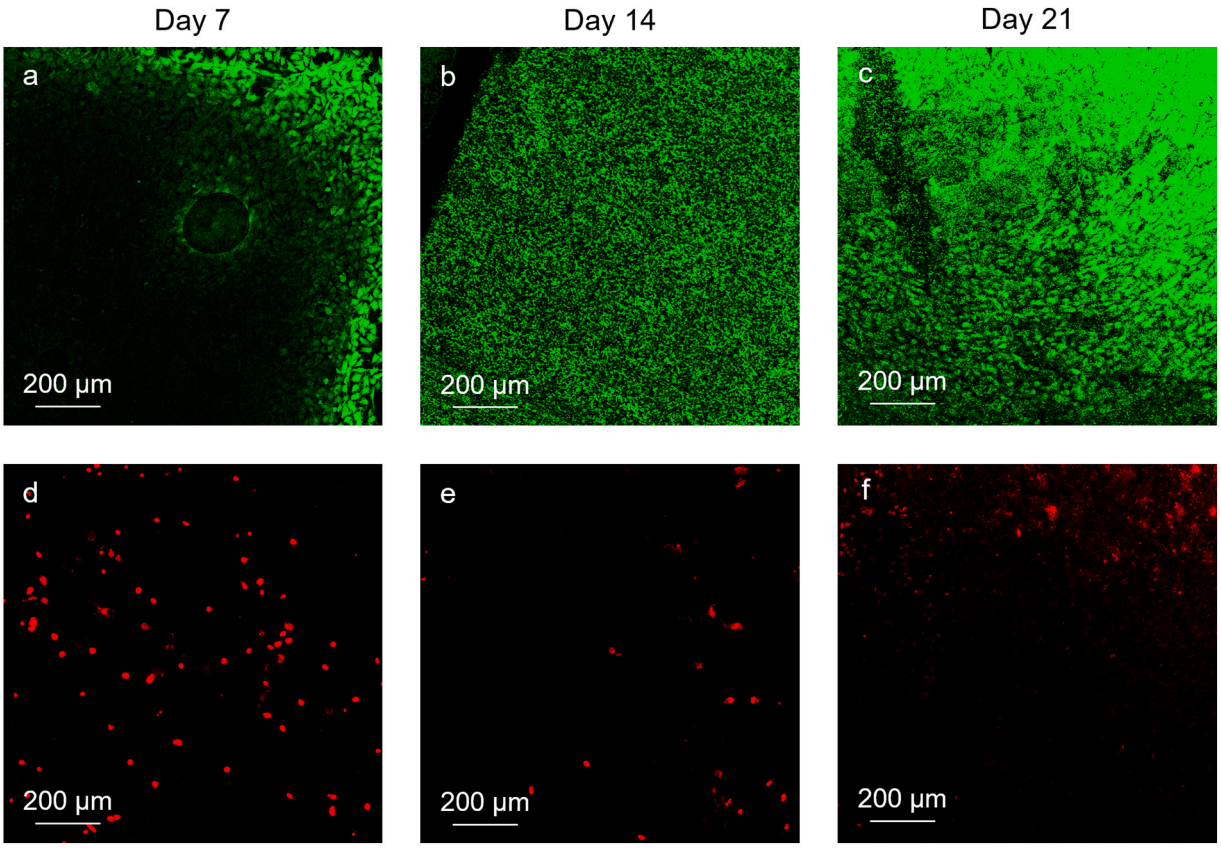

Fig. 5. Confocal micrographs for (a, b, c) live and (d, e, f) dead cells on the surface of BNT-6BT specimens coloured green and red respectively. (a, d) clusters of live cells with some cell death was observed after seven days; (b, e) cells had proliferated and increased in density on the piezoceramic surface by day 14; and (c, f) near-total saturation of the piezoceramic surface was seen by day 21 of culture. (For interpretation of the references to colour in this figure legend, the reader is referred to the web version of this article.)

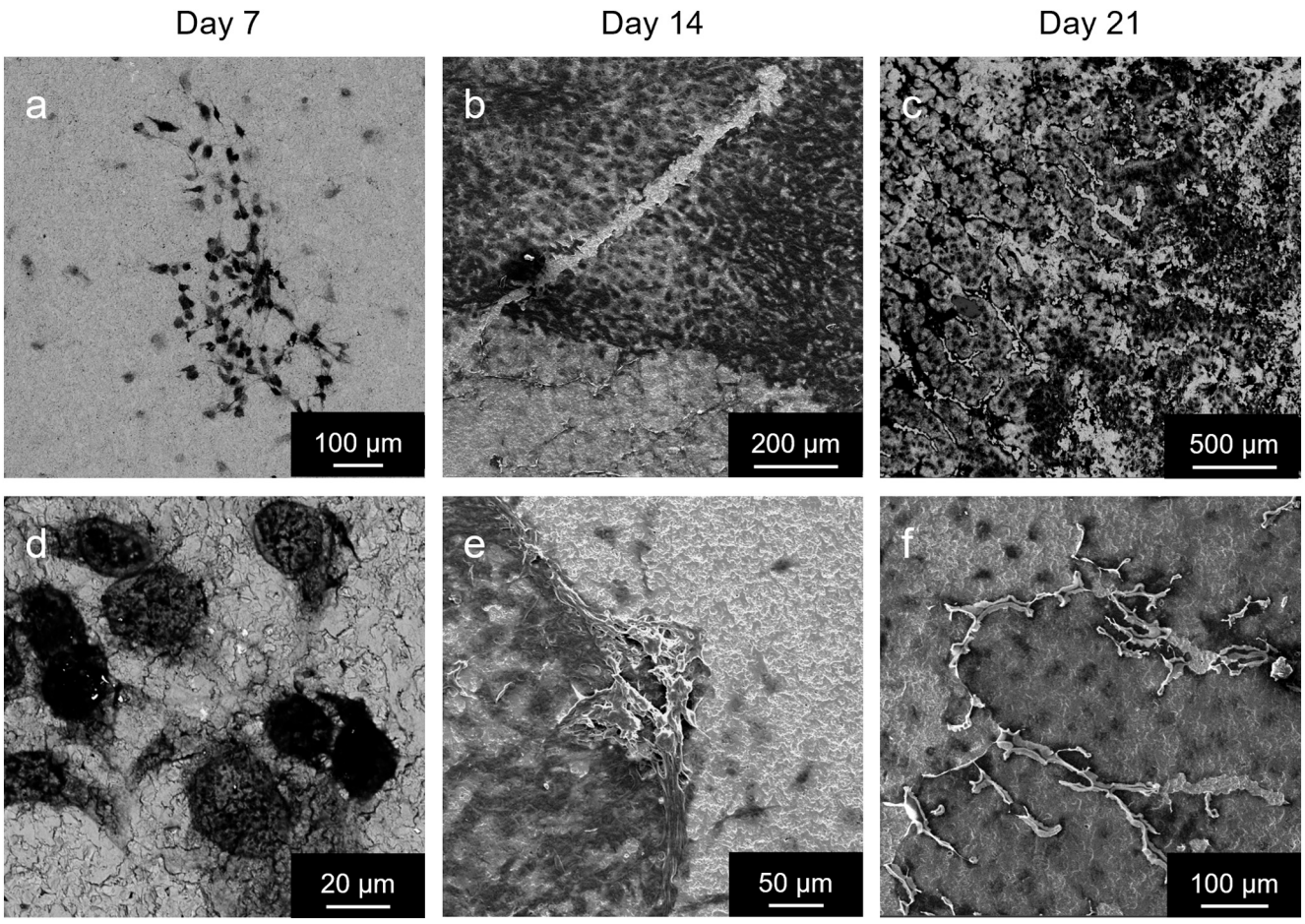

Fig. 6. Scanning electron micrographs (backscatter electron; beam energy: 10 keV; beam current: 300 pA) of MC3T3-E1 ongrowth onto BNT-6BT showing (a, d) clusters of flattened cells with lamellipodia at seven days, (b, e) widespread cell proliferation and small deposits of extracellular matrix by 14 days, and (c, f) dense, near-total coverage of the BNT-6BT surface with further deposition of extracellular matrix by 21 days.

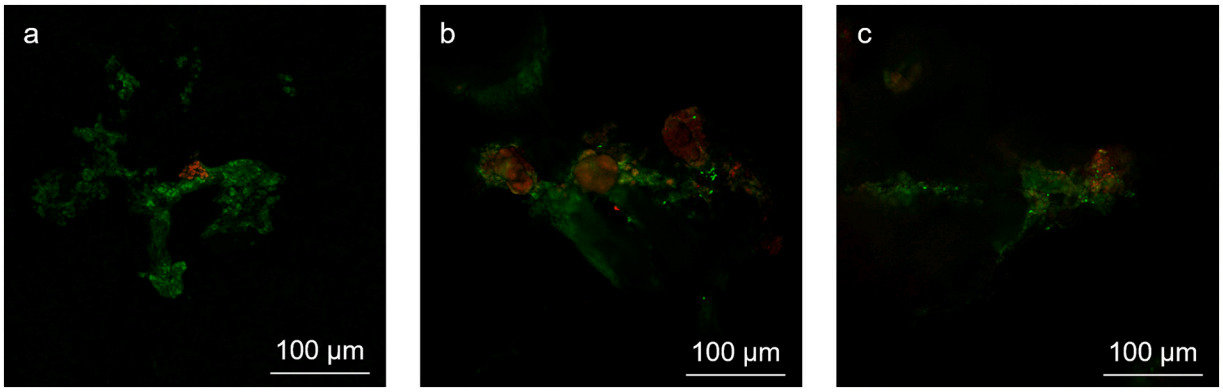

Fig. 7. Confocal micrographs of tissue stained with Calcein-AM/Ethidium homodimer (live cells: green; dead cells: red) after 28 days in ex vivo culture: (a) acellular organic deposits were observed on the implanted BNT-6BT specimens; (b) viable cells were observed on trabeculae adjacent to the BNT-6BT implant; and (c) cell viability was maintained on trabeculae in the bulk tissue (>2 mm from the BNT-6BT implant or any incised surface). (For interpretation of the references to colour in this figure legend, the reader is referred to the web version of this article.)

support the conclusions of the only previous biocompatibility study of BNT-6BT [33], which found no short-term harmful effect of BNT-6BT nanoparticles on lung carcinoma epithelial cells (A549). Neutral pH was maintained in both BNT-6BT and PZT specimens through 9 days of culture, which indicates no or minimal ion release from the solid-state materials during this time. Long-term ion release is an important concern for all piezoceramics: ion release has been reported in PZT [34], KNN [35] and BT [36], and similar behaviour should therefore be anticipated in BNT-6BT. Nonetheless, the ionic components of BNT-6BT are generally regarded as non-toxic: bismuth(III) compounds have several medical uses [37–39], though prolonged intake above the rate of excretion can cause encephalopathy through accumulation [40]; sodium is naturally occurring in the body; and barium titanate is otherwise considered highly biocompatible [41]. Additionally, ion release from

piezoceramics may terminate after an initial period as indicated by dissolution studies of BCZT, a BT-based piezoceramic, and could potentially be addressed by pre-conditioning the material prior to implantation [42].

Murine preosteoblasts (MC3T3-E1) proliferated on poled PIC700 when cultured in vitro with some evidence of extracellular matrix formation, which suggests BNT-6BT is conducive to osseointegration. Proliferation in direct contact with PIC700 was 47 % slower than in blank media ($p < 0.001$): this result was expected as cell culture wells are treated to make their surfaces more hydrophilic and adherent for cells, while the ceramic materials were untreated and their surface topography was not optimised in this preliminary investigation. Specimens were also in static culture, which does not capture potentially beneficial bulk effects of piezoelectric transduction under physiological loading. Prior investigations of pure BNT found that MC3T3-E1 cell proliferation and bone-like apatite formation depended on polarity, which could be harnessed for the regeneration of bone tissues [43]. The piezoelectric coefficients found in our study BNT-6BT are an order of magnitude stronger than pure BNT, two or three orders of magnitude stronger than hydroxyapatite [44] and natural bone [45], and in near-parity with barium titanate. Whilst optimum piezoelectric coefficients for bone regeneration have not been identified, several BT-based materials have been studied in supraphysiological piezoelectric implants: BT implants [41], BT-based composites [46] and BT foams with hydroxyapatite coating [47] have been shown to promote in vitro or in vivo bone growth and remodelling. Subsequently, BT-based piezoceramics have been integrated into biomedical implants using techniques including 3D printing [48–50], spray deposition [42], and electrospinning [51], though fabrication of complex electroactive scaffolds with high BT content remains a challenge. Given the manufacturability and biocompatibility demonstrated in this paper, BNT-6BT constitutes a strong candidate for the future production of electroactive scaffolds with high piezoceramic content and high piezoelectric coefficients. Similar additive techniques could be adopted to manufacture porous BNT-6BT scaffolds for piezoelectric bone stimulation.

5. Conclusion

While the figures of merit for BNT-6BT were 5–31 dB inferior to standard PZT-materials, the material was found to be non-cytotoxic and conducive to cell proliferation, and hence it could serve as a viable lead-free alternative for applications where moderate performance losses are tolerable, such as pulse-echo measurements and pressure sensing. BNT-6BT may also be a viable biomaterial for electroactive implants and implantable electronics without the need for hermetic sealing.

CRediT authorship contribution statement

Thomas A.G. Hall: Conceptualization, Methodology, Formal analysis, Data curation, Visualization, Investigation, Writing – original draft. **Konstantinos Theodoridis:** Methodology, Investigation, Writing – review & editing. **Stylianos Kechagias:** Methodology, Investigation, Writing – review & editing. **Nupur Kohli:** Methodology, Investigation, Writing – review & editing. **Christelle Denonville:** Methodology, Investigation, Writing – review & editing. **Per Martin Rørvik:** Methodology, Investigation, Writing – review & editing, Funding acquisition. **Frederic Cegla:** Supervision, Writing – review & editing. **Richard J. van Arkel:** Methodology, Supervision, Writing – review & editing, Funding acquisition.

Declaration of competing interest

Nothing to disclose.

Data availability

Data will be made available on request.

Acknowledgements

This research was financially supported by the Engineering and Physical Sciences Research Council (EPSRC) of UK Research and Innovation (EP/S022546/1; EP/R513052/1) and the Research Council of Norway (297561). All research animals had been euthanised for other unrelated research prior to transport and would have otherwise been disposed of as waste tissue. This research had no influence on the research, procedures, or euthanisation experienced by the living animals. Prior ethical approval was not required for this work, but it was declared by Dr. Richard van Arkel in his annual return in compliance with Imperial College London Policy on the Use of Animals in Research. The authors acknowledge Dr. Vegar Øygarden for electroding of TC-BNT-6BT samples and Henrik Ræder for valuable discussions.

Appendix A

Table A.1
Thickness-extension mode properties for PZT-based and lead-free piezoceramics materials from commercial and academic sources.

Family	Name	d_{33} (pC/N)	g_{33} (mV/m)	c_{33}^{D} (10^{10} N/m^2)	s_{33}^{E} (10^{-12} m^2/N)	$\varepsilon_{33}^{S}/\varepsilon_0$ (−)	k_t (−)	$tan\delta_E$ (10^{-4})	Q_M (−)	Reference
Soft PZT	5A	400	25.1	15.5	20.4	910	0.48	200	85	[53]
	5B	430	24.9	17.5	21.1	960	0.48	200	90	[53]
	5C	470	22.7	16.3	20.9	1140	0.51	150	80	[53]
	5D	580	22.2	16.6	23.0	1300	0.51	150	80	[53]
	5E	580	20.2	17.9	21.6	1480	0.52	200	85	[53]
	5H	640	19.8	15.0	23.5	1690	0.5	150	75	[53]
	5HD	680	19.9	16.8	23.8	1660	0.53	150	65	[53]
	5×	700	19.3	14.5	25.0	1880	0.53	200	65	[53]
	5XD	730	17.9	16.2	23.9	1710	0.55	200	60	[53]
	PIC151	500	21.5	15.7	19.4	1107	0.53	200	100	[52]
	PIC152	240	23.4	16.6	14.8	864	0.41	150	100	[52]
	PIC153	600	16.4	15.5	20.0	2105	0.49	300	50	[52]
	PIC155	360	27.9	15.8	19.3	782	0.48	250	80	[52]
	PIC255	400	25.0	15.4	19.0	864	0.47	200	80	[52]
	NCE51	443	26.3	16.2	21.3	823	0.50	150	80	[54]
Hard PZT	4A	145	41.6	17.4	12.8	240	0.48	30	1400	[53]
	4B	180	33.9	18.8	16.0	360	0.48	30	1300	[53]
	4C	220	32.9	17.9	16.9	430	0.48	40	1200	[53]
	4D	310	25.8	16.2	17.5	730	0.49	50	500	[53]
	4E	350	25.6	17.0	19.3	820	0.51	40	1000	[53]

(*continued on next page*)

Table A.1 (*continued*)

Family	Name	d_{33} (pC/N)	g_{33} (mV/m)	c_{33}^{D} (10^{10} N/m^2)	s_{33}^{E} (10^{-12} m^2/N)	$\varepsilon_{33}^{S}/\varepsilon_0$ (−)	k_t (−)	$tan\delta_E$ (10^{-4})	Q_M (−)	Reference
	4F	350	26.4	17.4	18.8	750	0.47	50	1500	[53]
	4G	340	24.1	16.7	17.5	840	0.49	50	1800	[53]
	8A	240	26.5	17.4	15.9	610	0.48	30	1000	[53]
	8B	260	24.6	17.8	15.2	690	0.48	20	1000	[53]
	PIC181	265	23.0	17.0	13.3	649	0.46	30	2000	[52]
	PIC184	220	22.4	15.8	13.7	546	0.44	30	400	[52]
	PIC144	225	23.3	16.6	14.3	640	0.48	30	1000	[52]
	PIC241	290	20.5	17.6	14.3	863	0.46	50	1200	[52]
	PIC300	155	20.9	16.3	12.0	614	0.43	30	1400	[52]
	NCE40	304	27.5	12.7	14.6	638	0.48	25	700	[52]
	NCE41	310	25.9	11.6	16.0	684	0.50	40	1400	[52]
	NCE81	255	28.0	12.7	15.0	551	0.47	17	1300	[52]
BNT	Pz46	18	9.2	–	–	211	0.20	40	2000	[82]
	BNT	95	25.2	–	–	–	–	320	–	[55]
	BNT	77	26.9	–	–	–	–	214	–	[56]
	BNT-6BT	125	24.3	–	10.0	538	0.53	130	–	[83]
	BNT-4BT	95	26.0	13.3	9.0	318	0.44	370	361	[58]
	BNT-6BT	148	28.5	13.6	9.2	457	0.40	480	330	[84]
	BNT-6BT	117	17.0	–	–	583	0.43	250	256	[57]
	BNT-6BT-La	125	9.0	–	–	626	0.38	450	182	[57]
	BNT-6BT-Nb	118	8.3	–	–	637	0.38	460	199	[57]
	BNT-6BT-Co	139	13.1	–	–	567	0.46	230	253	[57]
	BNT-6BT-La-Nb	135	9.2	–	–	640	0.38	440	127	[57]
	BNT-6BT-La-Co	127	11.2	–	–	622	0.38	210	263	[57]
	BNT-2BT	78	21.9	–	–	587	0.46	173	–	[59]
	BNT-4BT	87	22.1	–	–	592	0.45	207	–	[59]
	BNT-6BT	122	22.9	–	–	597	0.40	179	–	[59]
	BNT-8BT	112	15.0	–	–	628	0.42	204	–	[59]
	BNT-10BT	94	13.9	–	–	633	0.41	239	–	[59]
	BNT-BKT-BT	126	9.5	–	–	1063	0.50	600	40	[60]
KNN	Pz61	80	18.1	–	–	382	0.40	400	25	[61]
	KNN	110	26.3	–	–	319	0.45	300	–	[62]
	KNN	90	25.4	–	–	285	0.40	250	–	[63]
	Doped KNN	140	47.9	–	–	257	0.40	400	–	[63]
	KNN	127	29.0	21.4	10.1	306	0.46	150	240	[64]
	KNN-LS	265	21.7	15.9	15.0	830	0.46	200	40	[64]
	KNN-KCN	90	34.9	12.9	9.3	190	0.50	60	1500	[65]
	KNN-Ta	162	68.5	23.2	15.5	54	0.65	–	–	[65]
	KNN-LT	354	50.6	15.7	27.0	272	0.45	–	–	[65]
	KNN	95	23.8	–	–	–	–	–	–	[66]
	KNN-LT	200	39.6	–	–	–	–	–	–	[66]
	KNN-LN	235	–	–	–	–	0.48	–	–	[67]
	KNN-LN	170	49.2	–	–	–	–	275	–	[68]
	KNN-LN	314	53.7	–	–	–	–	–	–	[69]
	KNNS-BNKZ	490	–	–	–	1200	0.55	200	–	[70]
	KNNS-BNZH	380	21.4	12.7	16.8	975	0.48	200	200	[71]
	KNN-LS-BCZ	345	21.6	19.4	14.0	844	0.47	1000	~60	[72]
	KNN-LS-BZ	408	16.4	18.6	17.0	1628	0.39	1000	~30	[72]
BT	SM511	160	14.3	–	–	1000	0.32	50	1000	[73]
	BT	135	13.8	19.5	9.3	880	0.40	50	500	[53]
	BT	160	11	–	–	1279	0.26	50	1300	[74]
	BT-Li	260	16.8	–	–	–	–	–	357	[75]
	BT-LiF	270	10.6	–	–	–	–	120	–	[76]
	BCZT	620	–	–	–	–	–	–	–	[77]
	BCZT	572	13.4	–	–	–	–	150	125	[78]
	BCZT	390	3.9	16.2	6.5	2876	0.24	300	~1000	[79]
	BCZT-Zn	420	10.7	10.8	13.8	2788	0.42	–	135	[80]
	BCST	405	13.3	–	–	–	–	–	117	[81]

References

[1] B. İlik, A. Koyuncuoğlu, Ö. Şardan-Sukas, H. Külah, Thin film piezoelectric acoustic transducer for fully implantable cochlear implants, Sensors Actuators A Phys. 280 (2018) 38–46, https://doi.org/10.1016/J.SNA.2018.07.020.

[2] P. Jin, J. Fu, F. Wang, Y. Zhang, P. Wang, X. Liu, Y. Jiao, H. Li, Y. Chen, Y. Ma, X. Feng, A flexible, stretchable system for simultaneous acoustic energy transfer and communication, Sci. Adv. 7 (2021), https://doi.org/10.1126/SCIADV.ABG2507.

[3] J. Zhou, A. Kim, S.H. Song, B. Ziaie, An ultrasonically powered implantable micro-light source for localized photodynamic therapy, in: 2015 Transducers - 2015 18th Int. Conf. Solid-State Sensors, Actuators Microsystems, TRANSDUCERS 2015, 2015, pp. 876–879, https://doi.org/10.1109/TRANSDUCERS.2015.7181063.

[4] L. Tacchetti, W.A. Serdijn, V. Giagka, An ultrasonically powered and controlled ultra-high-frequency biphasic electrical neurostimulator, in: 2018 IEEE Biomed. Circuits Syst. Conf. BioCAS 2018 - Proc, Institute of Electrical and Electronics Engineers Inc., Cleveland, OH, USA, 2018, https://doi.org/10.1109/BIOCAS.2018.8584718.

[5] M.M. Ghanbari, D.K. Piech, K. Shen, S. Faraji Alamouti, C. Yalcin, B.C. Johnson, J. M. Carmena, M.M. Maharbiz, R. Muller, A sub-mm3 ultrasonic free-floating implant for multi-mote neural recording, IEEE J. Solid State Circuits 54 (2019) 3017–3030, https://doi.org/10.1109/JSSC.2019.2936303.

[6] J. Charthad, T.C. Chang, Z. Liu, A. Sawaby, M.J. Weber, S. Baker, F. Gore, S.A. Felt, A. Arbabian, A mm-sized wireless implantable device for electrical stimulation of peripheral nerves, IEEE Trans. Biomed. Circuits Syst. 12 (2018) 257–270, https://doi.org/10.1109/TBCAS.2018.2799623.

[7] C. Dagdeviren, B.D. Yang, Y. Su, P.L. Tran, P. Joe, E. Anderson, J. Xia, V. Doraiswamy, B. Dehdashti, X. Feng, B. Lu, R. Poston, Z. Khalpey, R. Ghaffari, Y. Huang, M.J. Slepian, J.A. Rogers, Conformal piezoelectric energy harvesting and storage from motions of the heart, lung, and diaphragm, Proc. Natl. Acad. Sci. U. S. A. 111 (2014) 1927–1932, https://doi.org/10.1073/PNAS.1317233111.

[8] A. Gjelsvik, Bone remodeling and piezoelectricity — I, J. Biomech. 6 (1973) 69–77, https://doi.org/10.1016/0021-9290(73)90039-0.

[9] A.H. Rajabi, M. Jaffe, T.L. Arinzeh, Piezoelectric materials for tissue regeneration: a review, Acta Biomater. 24 (2015) 12–23, https://doi.org/10.1016/J.ACTBIO.2015.07.010.

[10] S. Wang, C. Chen, J. Wang, C.-B.-W. Li, J. Zhou, Y.-X. Liu, Y.-Q. Jiang, L. Zhu, C. Li, W. Gong, W. Guo, X. Tang, F.-Z. Yao, K. Wang, Synergetic chemo-piezodynamic therapy of osteosarcoma enabled by defect-driven Lead-free piezoelectrics, Adv. Funct. Mater. 32 (2022) 2208128, https://doi.org/10.1002/adfm.202208128.

[11] P. Zhu, C. Yu, J. Shi, Piezocatalytic tumor therapy by ultrasound-triggered and BaTiO3-mediated piezoelectricity, Adv. Mater. 32 (2020) 20001976, https://doi.org/10.1002/adma.202001976.

[12] Agency for Toxic Substances and Disease Registry, Toxicological Profile for Lead (Update). https://www.atsdr.cdc.gov/toxprofiles/tp13.pdf, 2020 (accessed September 19, 2022).

[13] Directive 2011/65/EU, of the European Parliament and of the Council of 8 June 2011 on the restriction of the use of certain hazardous substances in electrical and electronic equipment (recast). http://data.europa.eu/eli/dir/2011/65/2021-11-01, 2011 (accessed May 30, 2022).

[14] J. Rödel, J.F. Li, Lead-free piezoceramics: status and perspectives, MRS Bull. 43 (2018) 576–580, https://doi.org/10.1557/MRS.2018.181.

[15] J. Wu, D. Xiao, J. Zhu, Potassium-sodium niobate lead-free piezoelectric materials: past, present, and future of phase boundaries, Chem. Rev. 115 (2015) 2559–2595, https://doi.org/10.1021/CR5006809.

[16] O. Tokay, M. Yazıcı, A review of potassium sodium niobate and bismuth sodium titanate based lead free piezoceramics, Mater. Today Commun. 31 (2022), 103358, https://doi.org/10.1016/J.MTCOMM.2022.103358.

[17] M. Acosta, N. Novak, V. Rojas, S. Patel, R. Vaish, J. Koruza, G.A. Rossetti, J. Rödel, BaTiO3-based piezoelectrics: fundamentals, current status, and perspectives, Appl. Phys. Rev. 4 (2017), 041305, https://doi.org/10.1063/1.4990046.

[18] Y. Saito, H. Takao, T. Tani, T. Nonoyama, K. Takatori, T. Homma, T. Nagaya, M. Nakamura, Lead-free piezoceramics, Nature. 432 (2004) 84–87, https://doi.org/10.1038/nature03028.

[19] M.E. Villafuerte-Castrejón, E. Morán, A. Reyes-Montero, R. Vivar-Ocampo, J. A. Peña-Jiménez, S.O. Rea-López, L. Pardo, Towards lead-free piezoceramics: facing a synthesis challenge, Materials (Basel) 9 (2016) 21, https://doi.org/10.3390/MA9010021.

[20] N. Zhang, T. Zheng, J. Wu, Lead-free (K,Na)NbO3-based materials: preparation techniques and piezoelectricity, ACS Omega 5 (2020) 3099–3107, https://doi.org/10.1021/ACSOMEGA.9B03658.

[21] H.C. Thong, C. Zhao, Z. Zhou, C.F. Wu, Y.X. Liu, Z.Z. Du, J.F. Li, W. Gong, K. Wang, Technology transfer of lead-free (K, Na)NbO3-based piezoelectric ceramics, Mater. Today 29 (2019) 37–48, https://doi.org/10.1016/J.MATTOD.2019.04.016.

[22] J. Zhao, N. Zhang, Y. Quan, G. Niu, W. Ren, Z. Wang, K. Zheng, Y. Zhao, Z.G. Ye, Evolution of mesoscopic domain structure and macroscopic properties in lead-free Bi0.5Na0.5TiO3-BaTiO3 ferroelectric ceramics, J. Appl. Phys. 129 (2021), 084103, https://doi.org/10.1063/5.0035466.

[23] J. Zhang, J. Zhao, Y. Quan, J. He, Y. Li, Z. Wang, K. Zheng, J. Zhuang, Z. Jiang, L. Wen, W. Ren, Fabrication and characterization of lead-free BNT-6BT ultrasonic transducers designed by an intelligent optimization algorithm, Crystals. 12 (2022) 1181, https://doi.org/10.3390/CRYST12081181/S1.

[24] British Standards Institution, Piezoelectric properties of ceramic materials and components, in: Methods of Measurement. Low Power, 2002 (https://doi.org/BS EN 50324-2:2002).

[25] T. Zheng, J. Wu, D. Xiao, J. Zhu, Recent development in lead-free perovskite piezoelectric bulk materials, Prog. Mater. Sci. 98 (2018) 552–624, https://doi.org/10.1016/J.PMATSCI.2018.06.002.

[26] J. Rödel, K.G. Webber, R. Dittmer, W. Jo, M. Kimura, D. Damjanovic, Transferring lead-free piezoelectric ceramics into application, J. Eur. Ceram. Soc. 35 (2015) 1659–1681, https://doi.org/10.1016/J.JEURCERAMSOC.2014.12.013.

[27] S. Priya, Criterion for material selection in design of bulk piezoelectric energy harvesters, IEEE Trans. Ultrason. Ferroelectr. Freq. Control 57 (2010) 2610–2612, https://doi.org/10.1109/TUFFC.2010.1734.

[28] S. Zhang, F. Li, X. Jiang, J. Kim, J. Luo, X. Geng, Advantages and challenges of relaxor-PbTiO3 ferroelectric crystals for electroacoustic transducers – a review, Prog. Mater. Sci. 68 (2015) 1–66, https://doi.org/10.1016/J.PMATSCI.2014.10.002.

[29] International Organization for Standardization, Biological Evaluation Of Medical Devices — Part 5: Tests for In Vitro Cytotoxicity, 2009 (doi:ISO 10993-5:2009).

[30] N. Kohli, K. Theodoridis, T.A.G. Hall, I. Sanz Pena, D.C.A. Gaboriau, R.J. van Arkel, Bioreactor analyses of tissue ingrowth, ongrowth and remodelling around implants: an alternative to live animal testing, Front. Bioeng. Biotechnol. 11 (2023), https://doi.org/10.3389/FBIOE.2023.1054391.

[31] L. Pardo, Á. García, F. Schubert, A. Kynast, T. Scholehwar, A. Jacas, J.F. Bartolomé, Determination of the PIC700 ceramic's complex piezo-dielectric and elastic matrices from manageable aspect ratio resonators, Materials (Basel) 14 (2021) 4076, https://doi.org/10.3390/MA14154076.

[32] N.G. Fenu, N. Giles-Donovan, M.R. Sadiq, S. Cochran, Full set of material properties of lead-free PIC 700 for transducer designers, IEEE Trans. Ultrason. Ferroelectr. Freq. Control 68 (2021) 1797–1807, https://doi.org/10.1109/TUFFC.2020.3044790.

[33] M. Esquivel-Gaon, S. Anguissola, D. Garry, A.D.C. Gallegos-Melgar, J.M. Saldaña, K.A. Dawson, A. De Vizcaya-Ruiz, L.M. Del Razo, Bismuth-based nanoparticles as the environmentally friendly replacement for lead-based piezoelectrics, RSC Adv. 5 (2015) 27295–27304, https://doi.org/10.1039/c5ra02151k.

[34] W.P. Chen, H.L.W. Chan, F.C.H. Yiu, K.M.W. Ng, P.C.K. Liu, Water-induced degradation in lead zirconate titanate piezoelectric ceramics, Appl. Phys. Lett. 80 (2002) 3587, https://doi.org/10.1063/1.1479205.

[35] S.W. Yu, S.T. Kuo, W.H. Tuan, Y.Y. Tsai, C.H. Su, Ion release from three lead-free piezoelectric ceramics and their physical and cytotoxicity characteristics, Mater. Lett. 65 (2011) 3522–3524, https://doi.org/10.1016/J.MATLET.2011.07.098.

[36] H.W. Nesbitt, G.M. Bancroft, W.S. Fyfe, S.N. Karkhanis, A. Nishijima, S. Shin, Thermodynamic stability and kinetics of perovskite dissolution, Nature. 289 (1981) 358–362, https://doi.org/10.1038/289358a0.

[37] A. Larsen, N. Martiny, M. Stoltenberg, G. Danscher, J. Rungby, Gastrointestinal and systemic uptake of bismuth in mice after Oral exposure, Pharmacol. Toxicol. 93 (2003) 82–90, https://doi.org/10.1034/J.1600-0773.2003.T01-1-930202.X.

[38] M. Bartoli, P. Jagdale, A. Tagliaferro, A short review on biomedical applications of nanostructured bismuth oxide and related nanomaterials, Materials (Basel) 13 (2020) 5234, https://doi.org/10.3390/MA13225234.

[39] J.C. Delchier, P. Malfertheiner, R. Thieroff-Ekerdt, Use of a combination formulation of bismuth, metronidazole and tetracycline with omeprazole as a rescue therapy for eradication of Helicobacter pylori, Aliment. Pharmacol. Ther. 40 (2014) 171–177, https://doi.org/10.1111/APT.12808.

[40] C. Borbinha, F. Serrazina, M. Salavisa, M. Viana-Baptista, Bismuth encephalopathy - a rare complication of long-standing use of bismuth subsalicylate, BMC Neurol. 19 (2019) 212, https://doi.org/10.1186/S12883-019-1437-9.

[41] J.B. Park, B.J. Kelly, G.H. Kenner, A.F. von Recum, M.F. Grether, W.W. Coffeen, Piezoelectric ceramic implants: in vivo results, J. Biomed. Mater. Res. 15 (1981) 103–110, https://doi.org/10.1002/JBM.820150114.

[42] K.K. Poon, Development of piezoelectric BCZT ceramics as electroactive bone implant materials, NTNU (2020). https://ntnuopen.ntnu.no/ntnu-xmlui/handle/11250/2653506 (accessed May 5, 2021).

[43] J.A. Hermann-Muñoz, J.A. Rincón-López, D.A. Fernández-Benavides, R. Detsch, J. M. Alvarado-Orozco, A.R. Boccaccini, J. Muñoz-Saldaña, In-vitro bioactivity and cytotoxicity of polarized (Bi0.5Na0.5)TiO3 ceramics as a novel biomaterial for bone repair, Mater. Lett. 275 (2020), 128078, https://doi.org/10.1016/j.matlet.2020.128078.

[44] C.C. Silva, D. Thomazini, A.G. Pinheiro, N. Aranha, S.D. Figueiró, J.C. Góes, A.S. B. Sombra, Collagen–hydroxyapatite films: piezoelectric properties, Mater. Sci. Eng. B 86 (2001) 210–218, https://doi.org/10.1016/S0921-5107(01)00674-2.

[45] A.J. Bur, Measurements of the dynamic piezoelectric properties of bone as a function of temperature and humidity, J. Biomech. 9 (1976) 495–507, https://doi.org/10.1016/0021-9290(76)90066-X.

[46] F. Jianqing, Y. Huipin, Z. Xingdong, Promotion of osteogenesis by a piezoelectric biological ceramic, Biomaterials. 18 (1997) 1531–1534, https://doi.org/10.1016/S0142-9612(97)80004-X.

[47] H. Zarkoob, S. Ziaei-Rad, M. Fathi, H. Dadkhah, Synthesis, characterization and bioactivity evaluation of porous barium titanate with nanostructured hydroxyapatite coating for biomedical application, Adv. Eng. Mater. 14 (2012) B322–B329, https://doi.org/10.1002/ADEM.201180091.

[48] C. Polley, T. Distler, R. Detsch, H. Lund, A. Springer, A.R. Boccaccini, H. Seitz, 3D printing of piezoelectric barium titanate-hydroxyapatite scaffolds with interconnected porosity for bone tissue engineering, Materials (Basel) 13 (2020) 1773, https://doi.org/10.3390/MA13071773.

[49] E. Mancuso, L. Shah, S. Jindal, C. Serenelli, Z.M. Tsikriteas, H. Khanbareh, A. Tirella, Additively manufactured BaTiO3 composite scaffolds: a novel strategy for load bearing bone tissue engineering applications, Mater. Sci. Eng. C 126 (2021), 112192, https://doi.org/10.1016/J.MSEC.2021.112192.

[50] Y. Yang, S. Peng, F. Qi, J. Zan, G. Liu, Z. Zhao, C. Shuai, Graphene-assisted barium titanate improves piezoelectric performance of biopolymer scaffold, Mater. Sci. Eng. C 116 (2020), 111195, https://doi.org/10.1016/J.MSEC.2020.111195.

[51] Y. Li, X. Dai, Y. Bai, Y. Liu, Y. Wang, O. Liu, F. Yan, Z. Tang, X. Zhang, X. Deng, Electroactive BaTiO3 nanoparticle-functionalized fibrous scaffolds enhance osteogenic differentiation of mesenchymal stem cells, Int. J. Nanomedicine 12 (2017) 4007, https://doi.org/10.2147/IJN.S135605.

[52] P.I. Ceramic, Ceramic Material Data. https://www.piceramic.com/en/products/piezoelectric-materials/, 2020.

[53] T.J. Piezo, Material Characteristics Tables for PZT Hard, Soft and PT/BT/PN Products, https://tjpiezo.com/wp-content/uploads/2021/10/Material-Characteristics-Tables-for-PZT-Hard-Soft-and-PTBTPN-Proudcts-08Oct2021.pdf, 2021.

[54] Noliac, NCE51 Specifications. http://www.noliac.com/products/materials/nce51/, 2022 (accessed June 28, 2022).

[55] M. Naderer, T. Kainz, D. Schütz, K. Reichmann, The influence of Ti-nonstoichiometry in Bi0.5Na0.5TiO3, J. Eur. Ceram. Soc. 34 (2014) 663–667, https://doi.org/10.1016/J.JEURCERAMSOC.2013.10.010.

[56] K. Kanie, Y. Numamoto, S. Tsukamoto, T. Sasaki, M. Nakaya, J. Tani, H. Takahashi, A. Muramatsu, Size-controlled hydrothermal synthesis of bismuth sodium and bismuth potassium Titanates fine particles and application to lead-free piezoelectric ceramics, Mater. Trans. 52 (2011) 1396–1401, https://doi.org/10.2320/MATERTRANS.M2010419.

[57] H.D. Li, C. De Feng, W.L. Yao, Some effects of different additives on dielectric and piezoelectric properties of (Bi1/2Na1/2)TiO3–BaTiO3 morphotropic-phase-boundary composition, Mater. Lett. 58 (2004) 1194–1198, https://doi.org/10.1016/J.MATLET.2003.08.034.

[58] L. Pardo, Á. García, K. Brebøl, E. Mercadelli, C. Galassi, Enhanced properties for ultrasonic transduction, phase transitions and thermal depoling in 0.96 (Bi0.5Na0.5)TiO3-0.04BaTiO3 submicrometre-structured ceramics, J. Phys. D. Appl. Phys. 44 (2011), 335404, https://doi.org/10.1088/0022-3727/44/33/335404.

[59] B.J. Chu, D.R. Chen, G.R. Li, Q.R. Yin, Electrical properties of Na1/2Bi1/2TiO3–BaTiO3 ceramics, J. Eur. Ceram. Soc. 22 (2002) 2115–2121, https://doi.org/10.1016/S0955-2219(02)00027-4.
[60] D.A. Fernandez-Benavides, A.I. Gutierrez-Perez, A.M. Benitez-Castro, M.T. Ayala-Ayala, B. Moreno-Murguia, J. Muñoz-Saldaña, Comparative study of ferroelectric and piezoelectric properties of BNT-BKT-BT ceramics near the phase transition zone, Mater. 11 (2018) 361, https://doi.org/10.3390/MA11030361.
[61] Meggitt, Pz61 Datasheet. https://www.meggittferroperm.com/wp-content/uploads/2017/10/201708_MSSDK_PZ61_Datasheet-Pz61.pdf, 2017 (accessed September 11, 2022).
[62] H. Birol, D. Damjanovic, N. Setter, Preparation and characterization of (K0.5Na0.5)NbO3 ceramics, J. Eur. Ceram. Soc. 26 (2006) 861–866, https://doi.org/10.1016/J.JEURCERAMSOC.2004.11.022.
[63] E. Ringgaard, T. Wurlitzer, Lead-free piezoceramics based on alkali niobates, J. Eur. Ceram. Soc. 25 (2005) 2701–2706, https://doi.org/10.1016/J.JEURCERAMSOC.2005.03.126.
[64] S. Zhang, R. Xia, T.R. Shrout, G. Zang, J. Wang, Characterization of lead free (K0.5Na0.5)NbO3–LiSbO3 piezoceramic, Solid State Commun. 141 (2007) 675–679, https://doi.org/10.1016/J.SSC.2007.01.007.
[65] S. Zhang, J.B. Lim, H.J. Lee, T.R. Shrout, Characterization of hard piezoelectric lead-free ceramics, IEEE Trans. Ultrason. Ferroelectr. Freq. Control 56 (2009) 1523–1527, https://doi.org/10.1109/TUFFC.2009.1215.
[66] Y. Guo, K.I. Kakimoto, H. Ohsato, (Na0.5K0.5)NbO3–LiTaO3 lead-free piezoelectric ceramics, Mater. Lett. 59 (2005) 241–244, https://doi.org/10.1016/J.MATLET.2004.07.057.
[67] Y. Guo, K.I. Kakimoto, H. Ohsato, Phase transitional behavior and piezoelectric properties of (Na0.5K0.5)NbO3–LiNbO3 ceramics, Appl. Phys. Lett. 85 (2004) 4121, https://doi.org/10.1063/1.1813636.
[68] Y. Hou, C. Wang, J. Zhao, H. Ge, M. Zhu, H. Yan, The fine-grained KNN–LN ceramics densified from nanoparticles obtained by an economical sol–gel route, Mater. Chem. Phys. 134 (2012) 518–522, https://doi.org/10.1016/J.MATCHEMPHYS.2012.03.026.
[69] P. Zhao, B.P. Zhang, J.F. Li, High piezoelectric d33 coefficient in Li-modified lead-free (Na,K)NbO3 ceramics sintered at optimal temperature, Appl. Phys. Lett. 90 (2007), 242909, https://doi.org/10.1063/1.2748088.
[70] J. Ou-Yang, B. Zhu, Y. Zhang, S. Chen, X. Yang, W. Wei, New KNN-based lead-free piezoelectric ceramic for high-frequency ultrasound transducer applications, Appl. Phys. A Mater. Sci. Process. 118 (2015) 1177–1181, https://doi.org/10.1007/S00339-015-9004-8.
[71] L. Qiao, G. Li, H. Tao, J. Wu, Z. Xu, F. Li, Full characterization for material constants of a promising KNN-based lead-free piezoelectric ceramic, Ceram. Int. 46 (2020) 5641–5644, https://doi.org/10.1016/J.CERAMINT.2019.11.009.
[72] B. Carreño-Jiménez, A. Reyes-Montero, R. López-Juárez, Complete set of ferro/piezoelectric properties of BaZrO3 and (Ba,Ca)ZrO3 doped KNLNS-based electroceramics, Ceram. Int. 48 (2022) 21090–21100, https://doi.org/10.1016/J.CERAMINT.2022.03.024.
[73] Steiner & Martins, Piezo Material Properties. https://www.steminc.com/piezo/PZ_property1.asp, 2022 (accessed September 12, 2022).
[74] APC International, BaTiO3 Specifications. https://www.americanpiezo.com/single-crystals-non-pzt-materials/bati03-specifications.html, 2022 (accessed September 12, 2022).
[75] T. Kimura, Q. Dong, S. Yin, T. Hashimoto, A. Sasaki, T. Sato, Synthesis and piezoelectric properties of Li-doped BaTiO3 by a solvothermal approach, J. Eur. Ceram. Soc. 33 (2013) 1009–1015, https://doi.org/10.1016/J.JEURCERAMSOC.2012.11.007.
[76] W.G. Yang, B.P. Zhang, N. Ma, L. Zhao, High piezoelectric properties of BaTiO3–xLiF ceramics sintered at low temperatures, J. Eur. Ceram. Soc. 32 (2012) 899–904, https://doi.org/10.1016/J.JEURCERAMSOC.2011.10.054.
[77] W. Liu, X. Ren, Large piezoelectric effect in Pb-free ceramics, Phys. Rev. Lett. 103 (2009), 257602, https://doi.org/10.1103/PHYSREVLETT.103.257602.
[78] Y. Tian, X. Chao, L. Wei, P. Liang, Z. Yang, Phase transition behavior and electrical properties of lead-free (Ba1−xCax)(Zr0.1Ti0.9)O3 piezoelectric ceramics, J. Appl. Phys. 113 (2013), 184107, https://doi.org/10.1063/1.4804173.
[79] A. Reyes-Montero, F. Rubio-Marcos, L. Pardo, A. Del Campo, R. López-Juárez, M. E. Villafuerte-Castrejón, Electric field effect on the microstructure and properties of Ba 0.9 Ca 0.1 Ti 0.9 Zr 0.1 O 3 (BCTZ) lead-free ceramics, J. Mater. Chem. A 6 (2018) 5419–5429, https://doi.org/10.1039/C7TA09798K.
[80] D.A. Tuan, V.T. Tung, L.T.U. Tu, T. Van Chuong, Synthesis and investigation of the physical properties of lead-free BCZT ceramics, Perovskite Piezoelectric Mater. (2019), https://doi.org/10.5772/INTECHOPEN.87935.
[81] M. Chen, Z. Xu, R. Chu, Y. Liu, L. Shao, W. Li, S. Gong, G. Li, Polymorphic phase transition and enhanced piezoelectric properties in (Ba0.9Ca0.1)(Ti1−xSnx)O3 lead-free ceramics, Mater. Lett. 97 (2013) 86–89, https://doi.org/10.1016/J.MATLET.2012.12.067.
[82] Meggitt, Pz46 Datasheet. https://www.meggittferroperm.com/wp-content/uploads/2017/10/201710_MSSDK_PZ46_Datasheet-Pz46.pdf, 2017 (accessed September 10, 2022).
[83] T. Takenaka, K.I. Maruyama, K. Sakata, (Bi1/2Na1/2)TiO3-BaTiO3 system for lead-free piezoelectric ceramics, Jpn. J. Appl. Phys. 30 (1991) 2236–2239, https://doi.org/10.1143/JJAP.30.2236/XML.
[84] L. Pardo, G. Álvaro, E. Mercadelli, C. Galassi, K. Brebøl, Field-induced phase transition and relaxor character in submicrometer-structured lead-free (Bi0.5Na0.5)0.94Ba0.06TiO3 piezoceramics at the morphotropic phase boundary, IEEE Trans. Ultrason. Ferroelectr. Freq. Control 58 (2011) 1893–1904, https://doi.org/10.1109/TUFFC.2011.2029.